Discharge simulation and volt-second consumption analysis during ramp-up on the CFETR tokamak*

Cheng-Yue Liu(刘成岳)[1,2], Bin Wu(吴斌)[2], Jin-Ping Qian(钱金平)[2], Guo-Qiang Li(李国强)[2], Ya-Wei Hou(侯雅巍)[3], Wei Wei(韦维)[1], Mei-Xia Chen(陈美霞)[1], Ming-Zhun Lei(雷明准)[2], and Yong Guo(郭勇)[2,†]

[1] *Physics Department, School of Electronic Science & Applied Physics, Hefei University of Technology, Hefei* 230601, *China*
[2] *Institute of Plasma Physics, Chinese Academy of Science, Hefei* 230026, *China*
[3] *University of Science and Technology of China, Hefei* 230031, *China*

(Received 10 November 2019; revised manuscript received 2 December 2019; accepted manuscript online 12 December 2019)

The plasma current ramp-up is an important process for tokamak discharge, which directly affects the quality of the plasma and the system resources such as volt-second consumption and plasma current profile. The China Fusion Engineering Test Reactor (CFETR) ramp-up discharge is predicted with the tokamak simulation code (TSC). The main plasma parameters, the plasma configuration evolution and coil current evolution are given out. At the same time, the volt-second consumption during CFETR ramp-up is analyzed for different plasma shaping times and different plasma current ramp rates $\mathrm{d}I_\mathrm{P}/\mathrm{d}t$ with/without assisted heating. The results show that the earlier shaping time and the faster plasma current ramp rate with auxiliary heating will enable the volt-second to save 5%–10%. At the same time, the system ability to provide the volt-second is probably 470 V·s. These simulations will give some reference to engineering design for CFETR to some degree.

Keywords: plasma current ramp-up, China Fusion Engineering Test Reactor, tokamak simulation code, volt-second consumption

PACS: 52.50.–b, 52.55.Fa, 52.65.–y **DOI:** 10.1088/1674-1056/ab610d

1. Introduction

The China Fusion Engineering Test Reactor (CFETR)[1] is a Chinese next-step tokamak, which is under engineering conceptual design. It will be an important facility to bridge from ITER to DEMO, which is envisioned to provide 200–1500 MW fusion power, $Q = 3$–30 and duty factor $\geqq$50%. The CFETR standard lower-single-null (LSN) configuration is shown in Fig. 1, which allows plasma to be flexibly shaped with elongation of 2, major radius of 7.2 m, minor radius of 2.2 m, and plasma current of 14 MA. The main parameters of the CFETR are listed in Table 1. The geometry parameters of coils are listed in Table 2. These coil packs are of width dR and height dZ, whose centers are at (R, Z). The superconducting coil system on the CFETR consists of eight central-solenoid (CS) coils, 6 poloidal-field (PF) coils, and one additional divertor-configuration coil (DC1). In Section 2, we briefly introduce the simulation model for the TSC code.[2] The CFETR ramp-up ohmic discharge modeling using the TSC code is presented in Section 3. The analysis of volt-second consumption and ability assessment for the CFETR ramp-up is described in Section 4 and finally a summary is given out in Section 5.

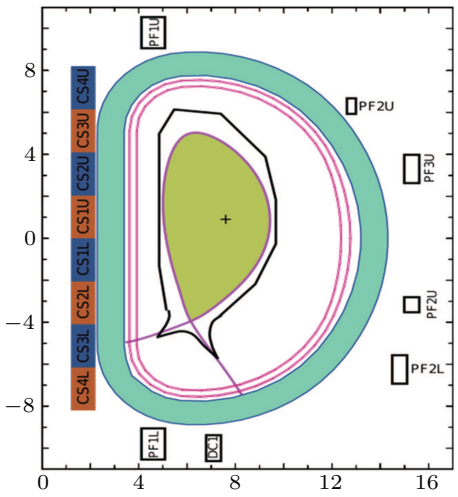

Fig. 1. CFETR standard LSN configuration.

Table 1. Main parameters of the CFETR.

Parameters	CFETR
Plasma current I_p	14 MA
Toroidal field B_t	6.5 T
Major radius R_0	7.2 m
Minor radius a	2.2 m
Elongation k	2.0
Plasma shape	LSN

*Project supported by the National Key Research and Development Program of China (Grant Nos. 2017YFE0300500 and 2017YFE0300501), the National Natural Science Foundation of China (Grant Nos. 11875290 and 11875253), and the Fundamental Research Funds for the Central Universities of China (Grant No. WK3420000004).

†Corresponding author. E-mail: yguo@ipp.ac.cn

Table 2. Geometric parameters of the CFETR poloidal field coils.

Coils	R/m	Z/m	dR	dZ	Turns
CS1U	1.70	1.025	1.0	2.05	738
CS2U	1.70	3.075	1.0	2.05	738
CS3U	1.70	5.125	1.0	2.05	738
CS4U	1.70	7.175	1.0	2.05	738
CS4L	1.70	−5.125	1.0	2.05	738
CS3L	1.70	−3.075	1.0	2.05	738
CS2L	1.70	−1.025	1.0	2.05	738
CS1L	1.70	−4.995	1.0	2.05	738
PF1U	4.60	9.80	1.1	1.5	448
PF2U	13.20	8.00	1.1	1.1	225
PF3U	15.73	3.15	1.1	1.1	225
PF1L	4.60	−9.80	1.1	1.5	448
PF2L	15.30	−6.90	1.1	1.1	225
PF3L	15.73	−3.15	1.1	1.1	225
DC1	7.10	−10.00	1.1	1.1	225

2. TSC simulation model

The tokamak simulation code (TSC) is a numerical model of an axisymmetric tokamak and is used to simulate the evolution of two-dimensional time-dependent free boundary plasma by advancing the MHD equations coupled with the external circuits. The code has been used not only to simulate normal discharges in the TFTR, ADITYA, EAST, but also to predict the future experiment in the ITER. The TSC code is coupled with transport calculations which solves the 1D flux surface averaged transport equations for energy, particles and current density utilizing predefined transport coefficients.[2,3]

The plasma force balance equation is

$$\frac{\partial \boldsymbol{m}}{\partial t} + \boldsymbol{F}_v(\boldsymbol{m}) = \boldsymbol{j} \times \boldsymbol{B} - \nabla p, \tag{1}$$

where $\boldsymbol{m}$ is plasma momentum density. According to Ohm's law and Faraday's law, evolutions for the poloidal flux and toroidal field functions can be expressed as follows:[4]

$$\frac{\partial \psi}{\partial t} + \frac{1}{\rho_0}(\nabla\phi \times \nabla A \cdot \nabla\varphi + \nabla\Omega \cdot \nabla\varphi) = k^2 \nabla\phi \cdot R, \tag{2}$$

$$\frac{\partial g}{\partial t} + x^2 \nabla \cdot \left[\frac{g}{\rho_0 x^2}(\nabla\phi \times \nabla A + \nabla\Omega) - \frac{\omega}{\rho_0 x^2}\nabla\phi \times \nabla\varphi - \nabla\phi \times R\right] = 0. \tag{3}$$

The surface-averaged particle and energy transport equations can be written as

$$\frac{\partial}{\partial t}N' = -\frac{\partial}{\partial \Phi}(N'\Gamma) + S_{\mathrm{N}}, \tag{4}$$

$$\frac{\partial}{\partial t}\sigma = \frac{2}{3}\left(\frac{\partial V}{\partial \Phi}\right)^{2/3}\left[V_L \frac{\partial K}{\partial \Phi} - \frac{\partial}{\partial \Phi}(Q_{\mathrm{i}} + Q_{\mathrm{e}}) + \frac{\partial V}{\partial \Phi}(S_{\mathrm{i}} + S_{\mathrm{e}})\right], \tag{5}$$

where S_{N}, S_{e}, S_{i}, and R_{e} are the external sources of particles, electron and ion energy and energy loss due to radiation. In the simulation of particle density transport, we force the density to have a profile given by

$$n_{\mathrm{e}}(\hat{\psi}, t) = n_{\mathrm{e}}^0(t)\left[1 - \hat{\psi}^{\beta_{\mathrm{N}}}\right]^{\alpha_{\mathrm{N}}} + n_{\mathrm{b}}(t), \tag{6}$$

where $\hat{\psi}$ is the normalized poloidal flux varying between 0 at the plasma center and 1 at the plasma edge, $n_{\mathrm{b}}(t)$ and $n_{\mathrm{e}}^0(t)$ are the densities at the plasma boundary and at the plasma center, respectively. In the simulation, we set $\alpha_{\mathrm{N}} = 1$ and $\beta_{\mathrm{N}} = 2$.

The poloidal magnet system in the CFETR are placed symmetrically about the device horizontal mid-plane. The primary purpose of central solenoid coils is to induce current in the plasma through transformer action, and poloidal field coils are used to control the shape and position of the plasma. The control system assumes that the current in each of the poloidal field coils is the sum of a preprogrammed current and a much smaller correction current, which is accomplished by letting the feedback current in each coil group be proportional to a flux difference between two observation points $(\boldsymbol{x_1}, \boldsymbol{x_2})$. The observation points are the coordinates at which the flux is measured for the feedback system. The location of these points is dependent on what the feedback system is to control and can vary in time. Thus, the current in each coil group is computed by

$$I_{\mathrm{w}}^k(t) = I_0^k(t) + I_{\mathrm{FB}}^k(t) = I_0^k(t) + \alpha_{\mathrm{p}}^k(\psi(\boldsymbol{x_1}) - \psi(\boldsymbol{x_2})), \tag{7}$$

where $I_{\mathrm{w}}^k(t)$ is desired current, $I_0^k(t)$ is the preprogrammed current, $I_{\mathrm{FB}}^k(t)$ is the feedback current, and α_{p}^k is the proportional gain.

3. The CFETR ramp-up discharge simulation

For the modeling CFETR ohmic discharge, the initial plasma equilibrium is computed by specifying the coil currents and plasma parameters at that time. After the initial equilibrium, it evolves in time. The initial plasma parameters include initial plasma current, plasma density, toroidal field and PF coil current, etc.,[5,6] as listed in Table 3.

Table 3. The main input parameters of CFETR simulation.

Time/s	1.0	5.00	14.000	42.0	70.0
CS1U/kA	51.26	48.76	43.15	25.67	8.20
CS2U/kA	51.34	49.27	44.62	30.13	15.64
CS3U/kA	50.59	48.76	44.64	31.81	18.99
CS4U/kA	49.45	47.40	42.80	28.49	14.18
CS4L/kA	49.45	48.44	46.18	39.16	32.15
CS3L/kA	50.59	50.02	48.74	44.75	40.77
CS2L/kA	51.34	48.92	43.45	26.46	9.46
CS1L/kA	51.26	48.13	41.10	19.22	−2.66
PF1U/kA	37.18	37.46	38.10	40.08	42.07
PF2U/kA	2.52	1.91	0.54	−3.73	−8.00
PF3U/kA	2.70	0.33	−4.54	−19.68	−34.83
PF1L/kA	37.18	37.85	39.36	44.05	48.74
PF2L/kA	1.52	−0.86	−6.22	−22.91	−39.59
PF3L/kA	2.70	2.22	1.58	−0.37	−2.34
DC1/kA	0.00	0.63	2.07	6.55	11.03
I_{p}/kA	200.0	1.0×10^3	2.8×10^3	8.4×10^3	14.0×10^3
$n_{\mathrm{e}}/10^{20}$ m^{-3}	0.05	0.062	0.100	0.275	0.450
BT/T	6.5	6.5	6.5	6.5	6.5

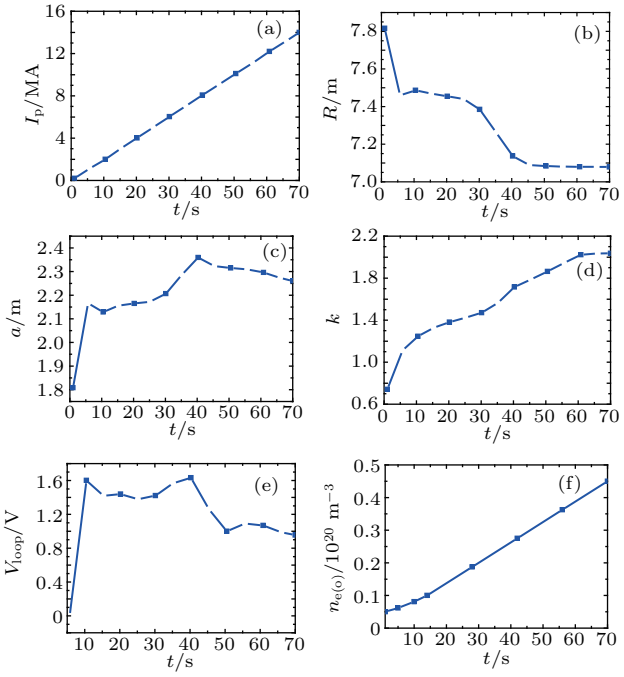

Fig. 2. CFETR discharge simulation during ramp-up: (a) plasma current, (b) plasma major radius, (c) plasma minor radius, (d) plasma elongation, (e) plasma loop voltage, and (f) plasma central electron density.

The plasma current reaches the flat-top 14 MA at 70 s from the initial 200 kA. It can be seen in Fig. 2 that the plasma is discharged in low field side with $R = 7.8$ m, $a = 1.8$ m. After 70 s ramp-up, the major radius, minor radius, elongation, loop voltage and central electron density are steady at $R = 7.1$ m, $a = 2.2$ m, $k = 2.0$, $V_{loop} = 1.0$ V, and $n_{e(o)} = 0.45 \times 10^{20}$ m^{-3}, respectively.

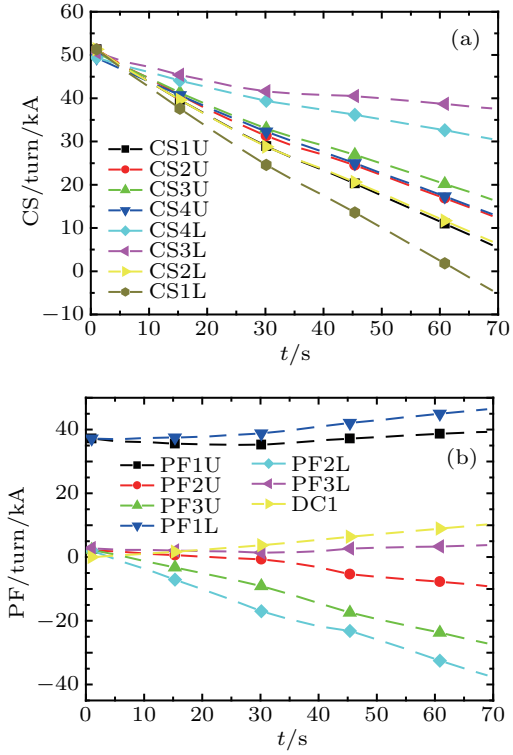

Fig. 3. CFETR coil current: (a) CS current evolution, (b) PF and DC1 coil current evolution.

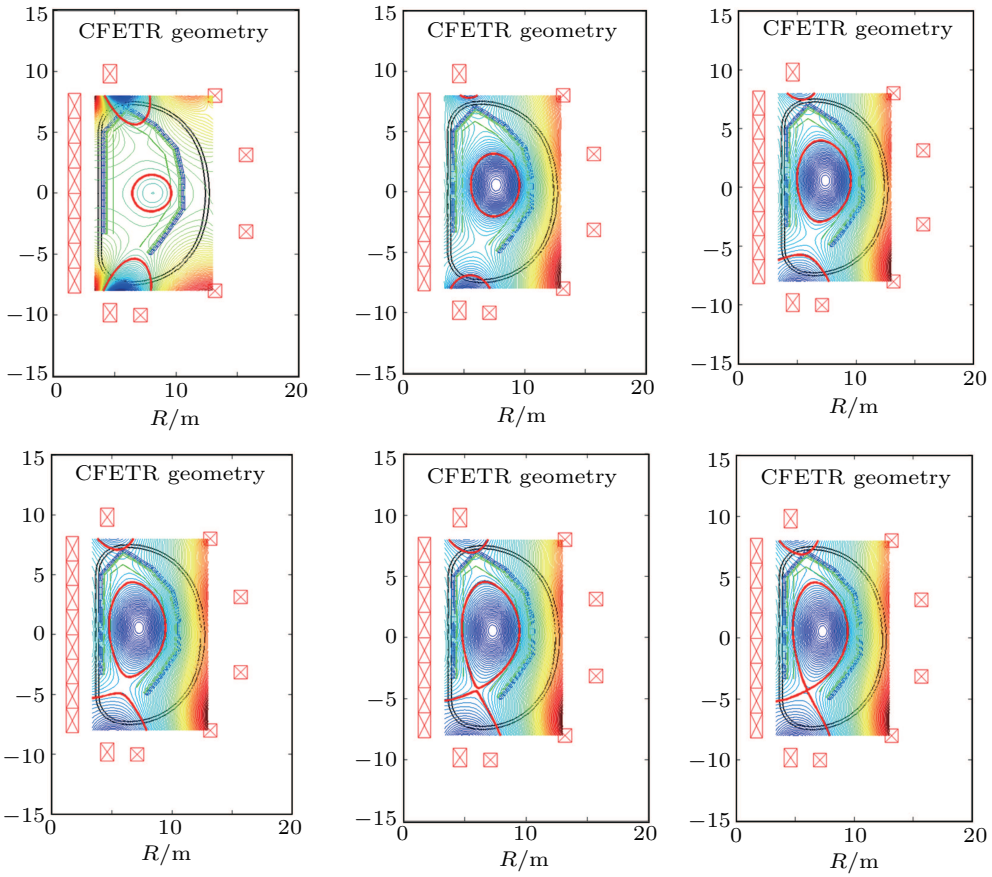

Fig. 4. CFETR plasma configuration evolution.

The temporal evolution of CS, PF, and DC1 currents is shown in Fig. 3. It can be seen that the CS coils maintain decreasing to afford plasma volt-second consumption and the PF1U and PF1L currents slightly climb up in order to shape the plasma. At the same time, Figure 4 gives the plasma magnetic configuration during ramp-up and describes the plasma configuration firstly forms limiter configuration and gradually evolves to divertor advanced configuration, which shows the stability of feedback control of PF current and configuration.[7,8]

4. The analysis of volt-second consumption in the discharge

For an ohmic tokamak discharge, the plasma current is driven only inductively and the volt-second variation afforded by the CS currents is limited, so we must make an efficient use of the available volt-second. The poloidal flux consumed by the plasma during the current ramp-up $\Delta\psi_{\rm total}$ can be divided into two parts in Eq. (8): an external part $\Delta\psi^{\rm ext}$ corresponding to the volt-second variation between the machine axis and the inside edge of the plasma and internal part $\Delta\psi^{\rm int}$ corresponding to the plasma boundary

$$\Delta\psi_{\rm total} = \Delta\psi^{\rm ext} + \Delta\psi^{\rm int}. \tag{8}$$

The external volt-second consumption is shown as

$$\Delta\psi^{\rm ext} = L^{\rm ext} I_{\rm p}, \tag{9}$$

where $L^{\rm ext}$ is plasma external inductance. The internal volt-second consumption is expressed as

$$\Delta\psi^{\rm int} = \Delta\psi^{\rm I} + \Delta\psi^{\rm R}. \tag{10}$$

An inductive volt-second $\Delta\psi^{\rm I}$ is required to establish the magnetic configuration and a resistive volt-second $\Delta\psi^{\rm R}$ to sustain the Ohmic dissipation. The internal volt-second consumption can be expressed with two methods: the axial method and the Poynting method.[9–11]

The axial method is based on flux conservation. In this method, the $\Delta\psi^{\rm R}$ and $\Delta\psi^{\rm I}$ are defined as the poloidal flux variation at the magnetic axis, and the poloidal flux variation at the plasma boundary and the plasma axis, respectively, expressed as follows:

$$\begin{aligned}
&\Delta\psi_{\rm A}^{\rm int} = \Delta\psi_{\rm A}^{\rm I} + \Delta\psi_{\rm A}^{\rm R},\\
&\Delta\psi_{\rm A}^{\rm I} = \Delta\psi(t)\,|_{x=1} - \Delta\psi(t)\,|_{x=0}\,,\\
&\Delta\psi_{\rm A}^{\rm R} = \Delta\psi(t)\,|_{x=0}\,,
\end{aligned} \tag{11}$$

where x is normalized poloidal flux. The Poynting method is based on energy conservation, and the plasma surface voltage is defined by

$$V_{\rm S} = -\frac{{\rm d}\psi_{\rm s}}{{\rm d}t}. \tag{12}$$

Thus, the internal volt-second consumption in the plasma boundary is expressed as

$$\begin{aligned}
&\Delta\psi_{\rm P}^{\rm int}({\rm t}) = -\Delta\psi_{\rm Surface} = \int {\rm d}t V_{\rm Surface} = \Delta\psi_{\rm P}^{\rm I}(t) + \Delta\psi_{\rm P}^{\rm R}(t),\\
&\Delta\psi_{\rm P}^{\rm I}(t) = \int I_{\rm p}^{-1}{\rm d}t \int {\rm d}V \partial/\partial t (B_{\rm p}^2/2\mu_0) = \mu_0 R_0 I_{\rm P} l_{\rm i}/2,\\
&\Delta\psi_{\rm P}^{\rm R}(t) = \int I_{\rm p}^{-1}{\rm d}t \int [{\rm d}V \boldsymbol{J}\cdot\boldsymbol{E} + {\rm Radiation}] = C_{\rm E}\mu_0 R_0 I_{\rm p},
\end{aligned} \tag{13}$$

where $l_{\rm i}$ and $C_{\rm E}$ are the plasma internal inductance and the $E_{\rm jima}$ coefficient, defined as

$$l_{\rm i} = 2\int B_{\rm p}^2 {\rm d}V/(R_0\mu_0^2 I_{\rm p}^2), \tag{14}$$

$$C_{\rm E} = \Delta\psi_{\rm p}^{\rm R}/(\mu_0 R_0 I_{\rm p}). \tag{15}$$

The modeling results of volt-second consumption with the axis method for the CFETR ramp-up are shown in Fig. 5. Figure 5(a) shows the total volt-second consumption (tot) 233 V·s from the initial ramping to the flat-top at 70 s, and Fig. 5(b) presents that resistive (R), inductive (I) and external volt-second (ext) consumptions are 18.5 V·s, 63 V·s and 143 V·s, respectively. At the same time, Fig. 6 gives the volt-second consumption with the Poynting method. From Fig. 6(a), resistive (R) and inductive (I) components are 39.02 V·s, and 43.05 V·s, respectively. Although the concrete components are different, the total internal volt-second consumptions are nearly equal, which shows the accuracy of volt-second consumption. The $E_{\rm jima}$ coefficient $C_{\rm E}$ is a function of time in Fig. 6(b) and is used to assess the resistive volt-second consumption. At the initial ramp-up, $C_{\rm E}$ is rapidly increase and indicates the increase of resistive volt-second. When approaching the flat-top, $C_{\rm E}$ tends to be steady.

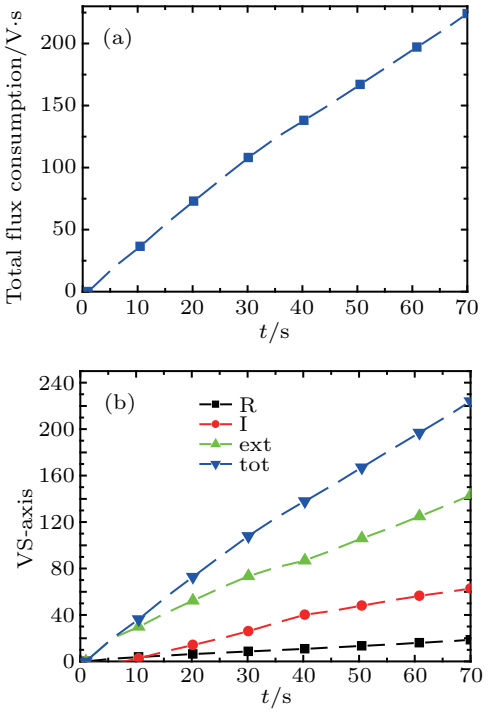

Fig. 5. CFETR volt-second consumption with the axis method: (a) total volt-second consumption evolution, (b) volt-second component evolution.

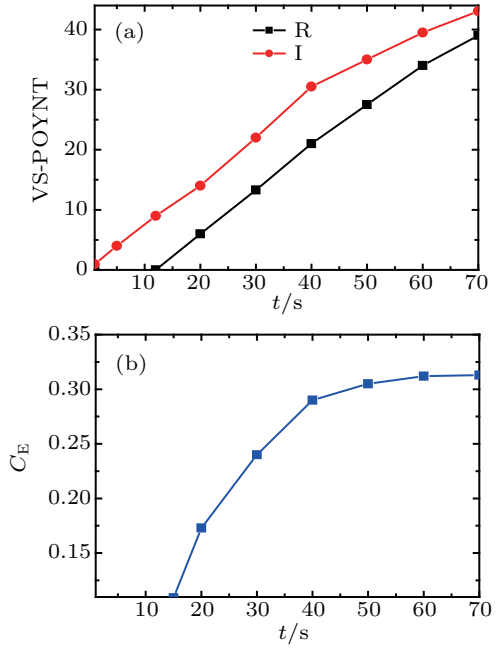

Fig. 6. CFETR volt-second consumption with the Poynting method: (a) internal component, (b) the E_{jima} coefficient C_E.

Because the volt-second is very essential for the CFETR steady operation in future, the optimization of volt-second consumption during plasma ramp-up is carried out from the angles of plasma shaping time point selection and plasma ramp rate dI_p/dt. The results shown in Fig. 7 are obtained by scanning CFETR plasma shaping time from 28 s to 70 s at the same $dI_p/dt \sim 0.2$ MA/s. As we can see that the internal volt-second consumptions are 76 V·s, 81 V·s and 96 V·s and the total volt-second consumptions are 220 V·s, 224 V·s and 243 V·s, respectively, at 28 s, 42 s and 70 s. The results show that earlier shaping with lower plasma current will be useful for saving volt-second consumption. Meanwhile, Figure 8 gives the results of scanning plasma current ramp rate dI_p/dt from 0.2 MA/s to 0.16 MA/s. We can see that the internal volt-second consumptions are 81 V·s, 88 V·s and 94 V·s and the total volt-second consumptions are 224 V·s, 231 V·s and 238 V·s, respectively at 70 s ($dI_p/dt \sim 0.2$ MA/s), 80 s ($dI_p/dt \sim 0.18$ MA/s) and 90 s ($dI_p/dt \sim 0.16$ MA/s). The results show that faster ramp-up can essentially decrease the flux consumption, especially for the resistive consumption.[12,13]

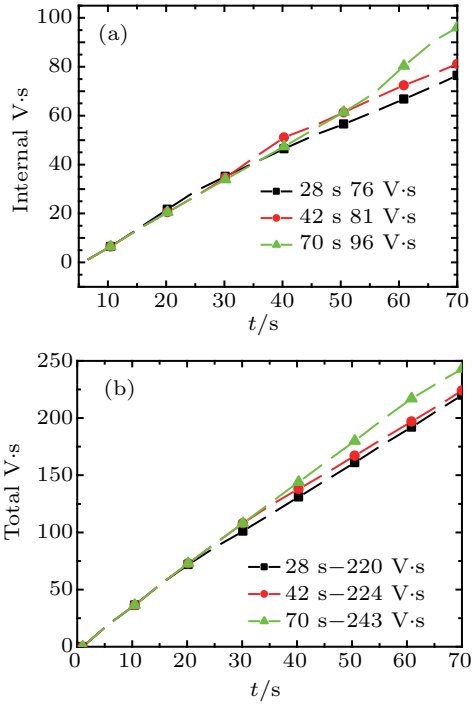

Fig. 7. Volt-second consumption at different plasma shaping times.

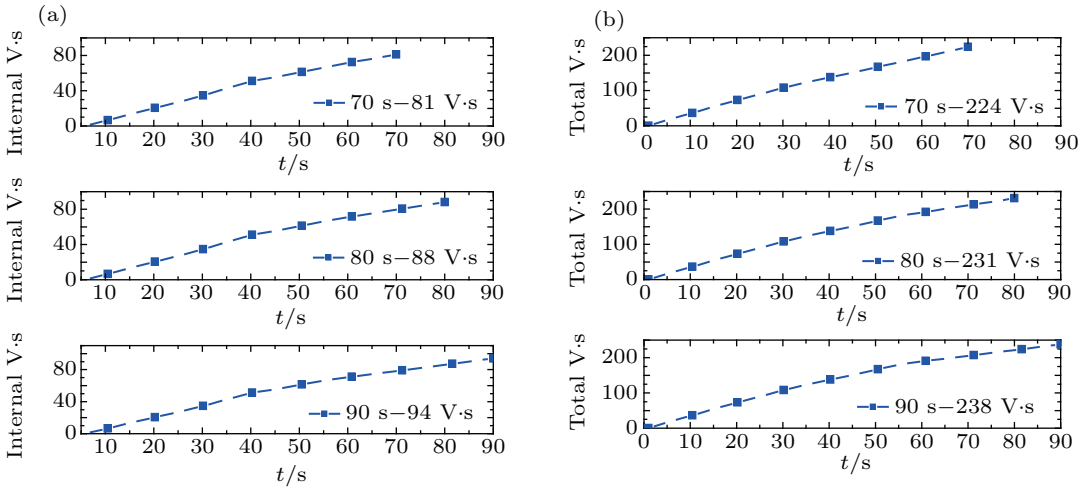

Fig. 8. Volt-second consumption at different plasma current ramp-up times.

The lower hybrid wave (LHW) assisting plasma ramping will also be used, as shown in Fig. 9. The simulations show that the internal and total volt-second consumptions are 81 V·s and 224 V·s under ohmic discharge. However, after LHW assisting plasma ramp-up, the internal and total volt-second consumptions are 65.9 V·s and 211 V·s, effectively decreased. Finally, the ability of volt-second afforded by the system is assessed with 470 V·s from the initial ramp-up to the entire plat-top duration not including plasma breakdown shown in Fig. 10.[14,15] At the same time, another similar result

about the CFETR volt-second ability assessment is obtained at 480 V·s, where the CS coils are treated as the infinite solenoid. The details are presented in Ref. [16] and all these simulations show the credibility of predicting CFETR volt-second ability.

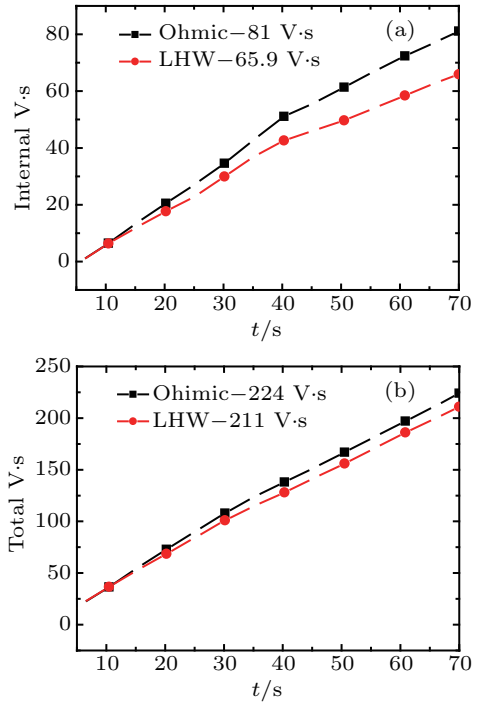

Fig. 9. Volt-second consumption with/without LHW assisted heating.

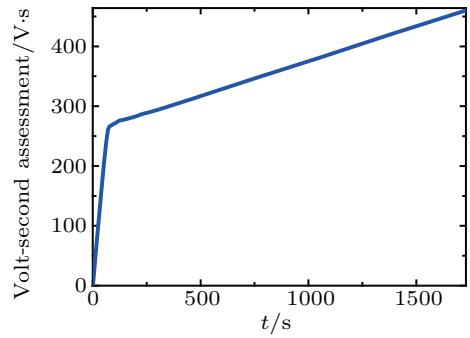

Fig. 10. The system volt-second ability assessment.

5. Conclusions

The CFETR ramp-up discharge is predicted with the TSC code and the plasma is finally steady at 14 MA with major radius $R = 7.1$ m, minor radius $a = 2.2$ m, elongation $k = 2$ and plasma central electron density $n_{e(o)} = 0.45 \times 10^{20}$ m^{-3}. The volt-second consumption is analyzed during ramp-up and the results show that the earlier shaping time and the faster plasma current ramp rate with auxiliary heating will enable volt-second to save 5%–10%. Finally, the system ability to provide the volt-second is probably 470 V·s.

Acknowledgments

The authors are grateful to PPPL for allowing to use the TSC code. Numerical simulations were carried out using the CFETR Integration Design Platform (CIDP) with the support of the Supercomputing Center of University of Science and Technology of China.

References

[1] Song Y T, Wu S T, Li J G, Wan B N, Wan Y X, Fu P, Ye M Y, Zheng J X, Lu K, Gao X G, Liu S M, Liu X F, Lei M Z, Peng X B and Chen Y 2014 *IEEE Trans. Plasma Sci.* **42** 503
[2] Jardin S C, Bell M G and Pomphrey N 1993 *Nucl. Fusion* **33** 371
[3] Wu B 2002 *Discharge Simulation of HT-7U Tokomak* (PhD dissertation) (Hefei: Institute of Plasma Physics, Chinese Academy of Sciences) (in Chinese)
[4] Jardin S C, Pomphrey N and Delucia J L 1986 *J. Comput. Phys.* **66** 481
[5] Guo Y, Xiao B J, Wu B and Liu C Y 2012 *Plasma Phys. Control. Fusion* **54** 085022
[6] Liu C Y, Wu B, Xiao B J and Shu S B 2008 *Plasma Sci. Technol.* **10** 8
[7] Jardin S C, Kessel C E and Pomphrey N 1994 *Nucl. Fusion* **34** 1145
[8] Wu Bin and Zhang C 2003 *Plasma Sci. Technol.* **5** 1625
[9] Menard J E, LeBlanc B, Sabbagh S A, Bell M, Bell R, Fredrickson E, Gates D, Jardin S, Kaye S, Kugel H, Maingi R, Maqueda R, Mueller D, Ono M, Paul S, Skinner C H, Stutman D and the NSTX Rearch Team 2001 *Nucl. Fusion* **41** 1197
[10] Ejima, S, Callis R W, Luxon J L, Stambaugh R D, Taylor T S and Wesley J C 1982 *Nucl. Fusion* **22** 1313
[11] Bandyopadhyay I, Ahmed S M, Atrey P K, Bhatt S B, Bhattacharya R, Chaudhury M B, Deshpande S P, Gupta C N, Jha R, Shankar J Y, Kumar V, Manchanda R, Raju D, Rao C V S, Vasu P and ADITYA Team 2004 *Plasma Physical and Controlled Fusion* **46** 1443
[12] Kessel C E, Giruzzi G, Sips A C C, Budny R V, Artaud J F, Basiuk V, Imbeaux F, Joffrin E, Schneider M, Murakami M, Luce T, Holger S J, Oikawa T, Hayashi N, Takizuka T, Ozeki T, Na Y S, Park J M, Garcia J and Tucillo A A 2007 *Nucl. Fusion* **47** 1274
[13] ITER Physics Basis Editors 1999 *Nucl. Fusion* **39** 2137
[14] Kim S H, Bulmer R H, Campbell D J, Casper T A, LoDestro L L, Meyer W H, Pearlstein L D and Snipes J A 2016 *Nucl. Fusion* **56** 126002
[15] Qiu Q L, Xiao B J, Guo Y, Liu L and Wang Y H 2017 *Chin. Phys. B* **26** 065205
[16] Zheng J X, Liu X F, Song Y T, Lu K, Du S S and Feng C 2019 *IEEE Trans. Appl. Supercond.* **29** 4600104